Computational Mechanics 27 (2001) 504–512 © Springer-Verlag 2001

A computational approach to the investigation of impact damage evolution in discontinuously reinforced fiber composites

H. K. Lee

Abstract A micromechanical damage constitutive model for discontinuous fiber-reinforced composites is developed to perform impact simulation. Progressive interfacial fiber debonding and a crack-weakened model are considered in accordance with a statistical function to describe the varying probability of damage. Emanating from a constitutive damage model for aligned fiber-reinforced composites, a micromechanical damage constitutive model for randomly oriented, discontinuous fiber-reinforced composites is developed. The constitutive damage model is then implemented into a finite element program DYNA3D to simulate the dynamic behavior and the progressive damage of composites. Finally, numerical simulations for a biaxial loading test and a four-point bend impact test of composite specimens are performed to validate the computational model and investigate impact damage evolution in discontinuous fiber-reinforced composite structures. Furthermore, in order to address the influence of Weibull parameter S_o on the damage evolution in composites, parametric analysis is carried out.

1 Introduction

Carbon fiber composites have been increasingly used for primary structural components in aerospace, automotive, and infrastructure applications. These materials have desirable engineering properties (e.g., high strength and stiffness, low density, long fatigue life, and high damage tolerance) and can be tailored to meet the intended function of the component. The success of the carbon fiber-reinforced composites as a mainstream automotive material depends on the development of the high-volume, high-reliability and quality, and cost-competitive manufacturing process that results in the material that meets and exceeds current automotive performance standards. The Programmable Powder Preform Process (P4) has been developed in recent years and has demonstrated its feasibility for automotive applications (Rondeau et al., 1999). P4 is a robotically articulated process in which discontinuous carbon fibers are deposited on the preform with precise spatial and orientation distributions.

From the performance standpoint, the greatest challenge posed by chopped carbon fiber composites is that they deform differently from the mild steel to which automotive designers are accustomed. This is the most apparent in vehicle crash where the impact-absorption components have to dissipate impact energy in a controlled and prescribed manner in order to protect vehicle occupants. The principal mechanisms by which crash energy is dissipated in composites are matrix cracking, fiber-matrix debonding, fiber-rupture, and delamination. The crashworthiness of automotive composite structures therefore requires an effective control over the damage processes and their sequence, the extent, and the interaction of these mechanisms, so that uncontrolled global failure is avoided (Waas and Quek, 1999).

It is well known that fiber-reinforced, organic matrix composites are very susceptible to impact damage, especially at low velocities. Low-velocity impact can cause significant damage inside the composites. Such damage is very difficult to detect and may cause significant reduction in the strength and stiffness of the materials. Furthermore, because of the natural tendency of the structure to acquire lower energy modes, both material and structural damage processes need to be well understood and modeled to simulate and eventually design the desirable sustained crush of the component. Hence, accurate analysis and simulation of the complete response of components and systems in discontinuous fiber-reinforced composites are essential and require accurate micromechanical constitutive models. The predictive analytical and numerical tools required to accurately evaluate and design carbon fiber automotive structures for crush do not currently exist. In order to successfully develop these tools, a damage constitutive model that incorporates various damage and deformation mechanisms for discontinuous fiber-reinforced composites is developed.

In our derivation, fibers are assumed to be elastic (prolate) spheroids that are randomly oriented in a polymer matrix. Penny-shaped cracks are assumed to remain at the same microcrack density during the deformations. After the interfacial debonding between the fibers and the matrix, these partially debonded fibers are regarded as equivalent, transversely isotropic inclusions. Governing micromechanical ensemble-volume averaged (homoge-

Received 29 April 2000

H. K. Lee
Department of Civil, Architectural, and Environmental Engineering, University of Miami, Coral Gables, FL 33124-0630
e-mail: hklee@miami.edu

This research was sponsored by the U.S. Department of Energy, Assistant Secretary for Energy Efficiency and Renewable Energy, Office of Transportation Technologies, Lightweight Materials Program, under contract DE-AC05-96OR22464 with Lockheed Martin Energy Research Corporation.

nized) field equations are constructed to derive the effective elastic moduli of aligned, discontinuous fiber-reinforced composites. Emanating from the constitutive damage model for aligned, discontinuous fiber-reinforced composites, a micromechanical damage constitutive model for randomly oriented, discontinuous fiber-reinforced composites is developed by employing the orientational averaging process (Lee and Simunovic, 2000). Progressive interfacial fiber debonding models are considered in accordance with a statistical function to describe the varying probability of fiber debonding. Only dilute or moderate fiber reinforced composites will be considered here.

The constitutive damage model is then implemented into a finite element program DYNA3D using a user-defined material subroutine to simulate the dynamic behavior and the progressive damage of composite materials. Finally, numerical simulations for a biaxial loading test and a four-point bend impact test of composite specimens are carried out to investigate impact damage evolution and examine whether the implemented computational model is able to predict the experimentally obtained response. In addition, parametric analysis is carried out to address the influence of Weibull parameter S_o on the damage evolution in composites.

2
A damage constitutive model for discontinuous fiber-reinforced composites

When a three-phase composite containing aligned, randomly dispersed, perfectly bonded fibers and penny-shaped cracks (see Fig. 1a) is subjected to remote tensile loading, some fibers may experience partial debonding on

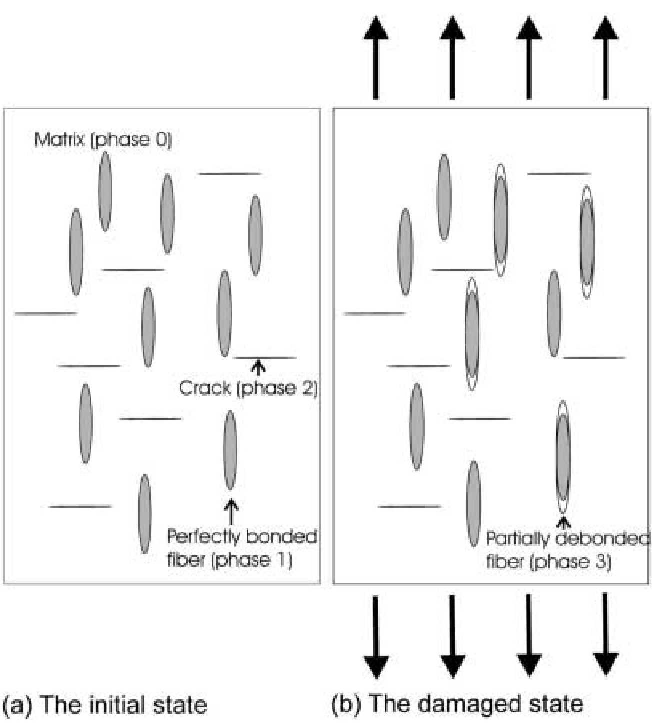

Fig. 1. A schematic diagram of aligned fiber composites subjected to uniaxial tension

the top and bottom of the interfaces between the matrix and fibers as deformations proceed (see Fig. 1b). The composite becomes a four-phase material, consisting of a ductile matrix (phase 0) with bulk modulus κ_0 and shear modulus μ_0; perfectly bonded fibers (phase 1) with bulk modulus κ_1 and shear modulus μ_1; penny-shaped cracks (phase 2); and partially debonded fibers (phase 3). The partially debonded fibers will lose their load-carry capacity, but they are still able to transmit internal stresses into matrix through the bonded portion. Following Zhao and Weng (1996, 1997) and Ju and Lee (2000), a partially debonded fiber can be replaced by an equivalent, perfectly bonded fiber that possesses yet unknown transversely isotropic moduli. The transverse isotropy of the equivalent fiber can be determined in such a way that (a) its tensile and shear stresses will always vanish in the debonded direction, and (b) its stresses in the bonded directions exist because the fiber is still able to transmit stresses to the matrix on the bonded surfaces (see Fig. 3.1 in Lee (1998)). Penny-shaped cracks are assumed to remain at the same microcrack density during the deformations.

Governing micromechanical ensemble-volume averaged field equations for linear elastic composites containing arbitrarily non-aligned and/or dissimilar ellipsoidal inclusions were derived by Ju and Chen (1994a). A normalization procedure was employed to render absolutely convergent integrals. For a multi-phase composite, the volume-averaged strain tensor $\bar{\boldsymbol{\epsilon}}$ assuming no interaction among constituents reads

$$\bar{\boldsymbol{\epsilon}} = \boldsymbol{\epsilon}^o + \sum_{r=0}^{n} \sum_{s=0}^{n} \phi_r \phi_s \mathbf{S}^{rs} : \bar{\boldsymbol{\epsilon}}_r^* \tag{1}$$

where $\boldsymbol{\epsilon}^o$ is the uniform strain field induced by far-field loads for a homogeneous matrix material only; n denotes the number of inclusion phases of different material properties (excluding the matrix); ϕ_r represents the volume fraction of the r-th phase inclusion; the fourth-rank tensor $\mathbf{S}^{rs}$ (r, s = phase numbering indices), which is related to renormalized integrals, is given in Eq. (12) of Ju and Chen (1994a); and $\bar{\boldsymbol{\epsilon}}_r^*$ signifies eigenstrain of r-th phase and is given by

$$\bar{\boldsymbol{\epsilon}}_r^* = -(\mathbf{A}_r + \mathbf{S}_r)^{-1} : \boldsymbol{\epsilon}^o \tag{2}$$

in which the fourth-rank tensor $\mathbf{A}_r$ is defined as

$$\mathbf{A}_r \equiv (\mathbf{C}_r - \mathbf{C}_0)^{-1} \cdot \mathbf{C}_0 \tag{3}$$

Here, $\mathbf{C}_r$ is the elasticity tensor of the r-phase. Eshelby's tensor of a spheroidal inclusion $\mathbf{S}_r$ for r-th phase inclusion was previously derived by Lee and Simunovic (2001); see Eqs. (19)–(26) therein.

The ensemble-volume averaged stress field $\bar{\boldsymbol{\sigma}}$ for a multi-phase composite was also derived by Ju and Chen (1994a) as

$$\bar{\boldsymbol{\sigma}} = \mathbf{C}_0 : \left[\bar{\boldsymbol{\epsilon}} - \sum_{r=1}^{n} \phi_r \bar{\boldsymbol{\epsilon}}_r^* \right] \equiv \mathbf{C}_* : \bar{\boldsymbol{\epsilon}} \tag{4}$$

Eq. (1) together with Eqs. (2) and (4) renders the following effective stiffness tensor for a multi-phase composite medium:

$$\mathbf{C}_* = \mathbf{C}_0 \cdot \left[\mathbf{I} + \sum_{r=1}^{n} \left\{ \phi_r (\mathbf{A}_r + \mathbf{S}_r)^{-1} \times \left[\mathbf{I} - \sum_{r=0}^{n} \sum_{s=0}^{n} \mathbf{S}^{rs} (\mathbf{A}_r + \mathbf{S}_r)^{-1} \phi_r \phi_s \right]^{-1} \right\} \right] \quad (5)$$

where $\mathbf{I}$ is the fourth-rank identity tensor.

Unidirectionally aligned penny-shaped microcracks can be regarded as the limiting case of unidirectionally aligned spheroidal voids with the aspect ratio $\alpha_3 \to 0$ (see Fig. 2). That is, one can collapse one axis of a spheroidal microvoid to recover a penny-shaped microcrack. In our derivation, fibers are assumed to be elastic prolate $(a_1 > a_2 = a_3)$ spheroids that are initially perfectly bonded in the matrix. Penny-shaped microcracks are regarded as oblate $(a_1 < a_2 = a_3)$ spheroids and remain the same volume fraction during the deformations. Furthermore, fibers and penny-shaped microcracks are assumed to be aligned; therefore, Eq. (5) can be simplified as

$$\mathbf{C}_* = \mathbf{C}_0 \cdot \left[\mathbf{I} + \sum_{r=1}^{n} \left\{ \phi_r (\mathbf{A}_r + \mathbf{S}_r)^{-1} \cdot [\mathbf{I} - \phi_r \mathbf{S}_r \cdot (\mathbf{A}_r + \mathbf{S}_r)^{-1}]^{-1} \right\} \right] \quad (6)$$

Accordingly, in the case of aligned (in the x_1-direction) crack-weakened, chopped fiber composites, the effective elastic stiffness tensor $\mathbf{C}_*$ can be explicitly derived as

$$\mathbf{C}_* = \tilde{F}_{ijkl}(\tau_1, \tau_2, \tau_3, \tau_4, \tau_5, \tau_6) \quad (7)$$

where the definition of fourth-rank tensor $\tilde{\mathbf{F}}$ is given in Eq. (2) of Lee and Simunoviv (2000) and the inverse and product of a fourth-rank tensor $\tilde{\mathbf{F}}$ are given in the appendix of Ju and Chen (1994b). The components $\tau_1, \ldots, \tau_6$ are given in the appendix.

Assuming all fibers and microcracks in the composite changed from aligned array to three-dimensional random array, the effective elastic moduli of crack-weakened, (randomly oriented) chopped fiber composites can be obtained by applying the orientational averaging process proposed by Lee and Simunovic (2000). Assuming the uniform distribution of overall strains, the effective elastic stiffness tensor $\subset \mathbf{C}_* \supset$ in Eq. (7) is averaged over all orientations as

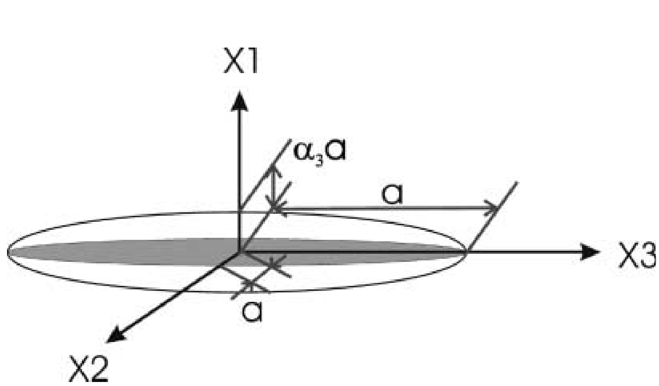

Fig. 2. Schematic description of a spheroidal inclusion

$$\subset C_* \supset = \frac{1}{2\pi} \int_0^{\pi} \int_0^{\pi} l_{mi} l_{nj} (C_*)_{mnpq} l_{pk} l_{ql} \sin\theta \, d\theta \, d\phi = \mathscr{C}_1 \delta_{ij} \delta_{kl} + \mathscr{C}_2 (\delta_{ik}\delta_{jl} + \delta_{il}\delta_{jk}) \quad (8)$$

with

$$\mathscr{C}_1 = \frac{1}{15}[\tau_1 + 5(\tau_3 + \tau_4 + 3\tau_5)] \quad (9)$$

$$\mathscr{C}_2 = \frac{1}{15}[\tau_1 + 10\tau_2 + 15\tau_6] \quad (10)$$

where l_{ij} denotes the directional cosine between i-th primed and jth unprimed axes. More detail of the orientational process can be found in Lee and Simunovic (2000).

3
Weibull function for damage evolution

The progressive, interfacial debonding may occur under increasing deformations and influence the overall stress–strain behavior of composites. After the interfacial debonding between fibers and the matrix, the debonded fibers lose the load-carrying capacity in the debonded direction and are regarded as partially debonded fibers. In the constitutive relation it is assumed that the debonding of fibers is controlled by the stress of the fibers and the statistical behavior of the fiber-matrix interfacial strength as shown in Fig. 3. Further, we employ the hydrostatic tensile stress of fibers $(\sigma_f)_m$ as the controlling factor. The Weibull (1951) distribution is chosen among several probability distribution functions used frequently in engineering fields to model the assumed cumulative probability of the interfacial debonding in Fig. 3; see also, Tohgo and Weng (1994), and Zhao and Weng (1996, 1997).

We now turn to the problem of dealing with the Weibull statistical function. The Weibull probability density function (three-parameter function: a, b, and c) is defined as

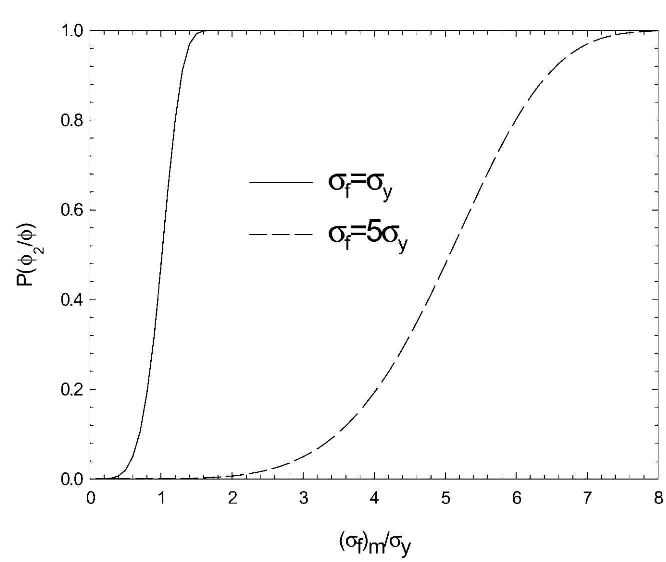

Fig. 3. Probability of normalized cumulative volume fraction of debonded fibers as a function of normalized interfacial bond strength

$$p(x) = \left(\frac{b}{a}\right)\left(\frac{x-c}{b}\right)^{a-1}\exp\left\{-\left(\frac{x-c}{b}\right)^{a}\right\} \tag{11}$$

subject to the following conditions

$$\begin{aligned} &c < x < +\infty \\ &a, b > 0, \quad c > -\infty \end{aligned} \tag{12}$$

The probability Pr that the random variable X will be between the two points on the real line x_a and x_b is

$$\Pr(x_a \le X \le x_b) = \int_{x_a}^{x_b} p(x)\mathrm{d}(x) \tag{13}$$

The probability distribution function $P(x)$ is the integral of the probability density function:

$$P(x) = \int_{-\infty}^{x} p(x)\mathrm{d}x = \Pr[X \le x] \tag{14}$$

where $P(x)$ is the probability that the random variable X will have a value equal to or less than x. The mean of X and its variance are

$$\bar{X} = c + b\Gamma\left[1 + \left(\frac{1}{a}\right)\right] \tag{15}$$

$$\sigma_x^2 = b^2\left\{\Gamma\left[1 + \left(\frac{2}{a}\right)\right] - \Gamma^2\left[1 + \left(\frac{1}{a}\right)\right]\right\} \tag{16}$$

in which the Gamma function $\Gamma(\cdot)$ is defined as

$$\Gamma(t) = \int_0^{\infty} y^{t-1}\exp(-y)\mathrm{d}y \tag{17}$$

Now let us consider applying the Weibull process mentioned above for progressive damage modeling. A Weibull's statistical function to describe the probability of fiber debonding (damage) at the level of hydrostatic tensile stress $(c < (\sigma_f)_m < \infty,\ c = 0)$ can be obtained by replacing a, b, and x in Eq. (11) with M, S_o, and $(\sigma_f)_m$, respectively.

$$p[(\sigma_f)_m] = \left(\frac{S_o}{M}\right)\left[\frac{(\sigma_f)_m}{S_o}\right]^{M-1}\exp\left\{-\left[\frac{(\sigma_f)_m}{S_o}\right]^{M}\right\} \tag{18}$$

where the hydrostatic tensile stresses of the fibers $(\sigma_f)_m = [(\sigma_{11})_f + (\sigma_{22})_f + (\sigma_{33})_f]/3$. The constants S_o and M in Eq. (18) are scale (Weibull modulus) and shape parameters of the Weibull function, respectively.

The Weibull probability distribution function for cumulative fiber debonding at the level of hydrostatic tensile stress reads

$$\begin{aligned} P_d[(\sigma_f)_m] &= \int_0^{(\sigma_f)_m} p[(\sigma_f)_m]\mathrm{d}(\sigma_f)_m \\ &= \int_0^{(\sigma_f)_m} \left(\frac{S_o}{M}\right)\left[\frac{(\sigma_f)_m}{S_o}\right]^{M-1}\exp\left\{-\left[\frac{(\sigma_f)_m}{S_o}\right]^{M}\right\} \\ &= 1 - \exp\left\{-\left[\frac{(\sigma_f)_m}{S_o}\right]^{M}\right\} \end{aligned} \tag{19}$$

Finally, the current partially debonded (damaged) fiber volume fraction ϕ_2 at a given level of $(\sigma_f)_m$ is given by

$$\phi_2 = \phi \cdot P_d[(\sigma_f)_m] = \phi \cdot \left\{1 - \exp\left[-\left(\frac{(\sigma_f)_m}{S_o}\right)^{M}\right]\right\} \tag{20}$$

where ϕ is the original fiber volume fraction. The (internal) stresses of fibers required for the initiation of interfacial debonding can be found in Ju and Lee (2000) and Lee and Simunovic (2001). Figure 4 shows the evolution of volume fraction of debonded fibers versus strains and illustrates the influence of Weibull modulus on the extent of damage.

Furthermore, with the Weibull distribution function, the relationship between average interfacial bond strength denoted by $\bar{\sigma}_f$ and the Weibull modulus S_o can be obtained through the Gamma function ($M = 5$)

$$\bar{\sigma}_f = S_o\Gamma\left(1 + \frac{1}{M}\right) = S_o\int_0^{\infty} x^{(1+\frac{1}{M})-1}\exp(-x)\mathrm{d}x = \frac{S_o}{1.09} \tag{21}$$

where the quality of the interfacial bond strength $\bar{\sigma}_f$ between fibers and the matrix is important in composite strengthening and interfacial debonding. It has been reported that the average interfacial bond strength $\bar{\sigma}_f$ in composites is related to the yield stress of composites σ_y (e.g., $\bar{\sigma}_f = 1 \sim 10\sigma_y$; see Goan and Prosen, 1969; Flom and Arsenault, 1986; and Ochiai and Osamura, 1988). Consequently, there are two ways to measure the Weibull modulus S_o: (a) experimental prediction: the value of S_o can be measured through the relationship between $\bar{\sigma}_f$ and S_o in Eq. (21) after direct experimental measurement of the interfacial bond strength $\bar{\sigma}_f$; (b) parametric evaluation:

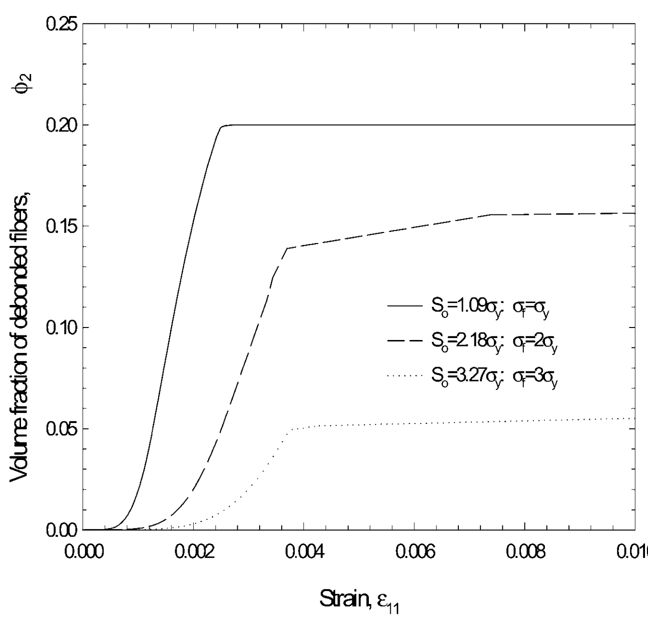

Fig. 4. The predicted evolution of volume fraction of debonded fibers versus strain

following the experimental observations mentioned above, the value of S_o can be chosen to yield some simple interfacial strength conditions in damage modeling as a parametric study. For example,

$$\bar{\sigma}_f = \sigma_y \rightarrow S_o = 1.09\sigma_y; \quad \text{weak interfacial strength}$$
$$\bar{\sigma}_f = 3\sigma_y \rightarrow S_o = 3.27\sigma_y; \quad \text{intermediate interfacial strength}$$
$$\bar{\sigma}_f = 10\sigma_y \rightarrow S_o = 10.9\sigma_y; \quad \text{strong interfacial strength.}$$

4 Finite element implementation and numerical simulations

The constitutive model derived is implemented into the nonlinear finite element code using a user-defined material subroutine to simulate the dynamic behavior and the progressive damage of the composite materials. While the implicit integration is chosen with an automatic time increment because it is not restricted to mildly nonlinear deformations or short response times, the explicit method is computationally attractive when the response time of interest is within an order of magnitude of the time it takes for a stress wave to travel through the shell thickness. Accordingly, the developed damage models are implemented into the explicit finite element code DYNA3D for impact simulation required a very small time step. The methodology used in this work is based on the well-known strain-driven algorithm in which the stress history is to be uniquely determined by the given strain history, mainly because of its computational efficiency in the framework of explicit time integration computer program DYNA3D.

Box 1 summarizes the iterative computational algorithm for the damage behavior of four-phase, discontinuous fiber-reinforced composites accounting for damage evolution. It renders a step-by-step flow chart for the computational procedure to determine the current damaged fiber volume fraction in accordance with the Weibull function for damage evolution in Sect. 3.

4.1 Numerical simulations for a biaxial test of cruciform shaped composite specimen

Planar biaxial tests were performed by Waas and Quek (1999) to gain insight into the constitutive behavior of damage induced composite materials. Towards reaching this goal, a number of biaxial tests with cruciform shaped specimens containing centrally located cutouts were carried out. Numerical simulations for the biaxial test are carried out to examine whether the implemented computational model is able to predict the experimentally obtained response. The geometry and loading conditions in this problem are symmetric along the x- and y-axes. The composite specimen is loaded proportionally with the rate of 30 lb/s (130 N/s) in biaxial compression and tension in the ratio of 1:1. A computational model of the cruciform shaped composite specimen and loading conditions are shown in Fig. 5. The material properties, volume fraction of fibers, aspect ratio of fibers, and Weibull parameters involving these simulations are $E_0 = 3.0$ GPa, $\nu_0 = 0.35$, $E_1 = 72.0$ GPa, $\nu_1 = 0.17$, $\phi_1 = 0.3$, $\alpha = 5.0$, $S_o = 165$ MPa, and $M = 4.0$. The default DYNA3D shell element formulation based on Belyschko–Tsay theory is utilized for modeling the composite specimen.

Figure 6 shows the sequence of damage contours during biaxial loading, representing the growth of damage zone due to the advancing damage one emanating from the edges of the cutout. Time history plots for the damage index ϕ_3 (current volume fraction of damaged fibers) around the cutout of the composite specimen are shown in Fig. 7. Figures 6 and 7 exhibit the damage initiation and evolution along the x- and y-axes around the cutout, which correspond with Waas and Quek's (1999) observations. These simulations can be used for predicting the direction and rate of damage propagation during biaxial test.

Box 1. Iterative algorithm for progressive damage model

(i) Estimate Weibull parameters: $S_o,\ M$

(ii) Initialize: set $z = 0$; $(\phi_1)^{(0)}_{n+1} = (\phi_1)_n,\ (\phi_3)^{(0)}_{n+1} = (\phi_2)_n$

(iii) Compute:

Effective moduli: $(E_*)^{(z)}_{n+1},\ (\nu_*)^{(z)}_{n+1}$;

Internal stresses of fibers: $[(\bar{\sigma}_m)_1]^{(z)}_{n+1}$

(iv) Compute the Weibull probability distribution function:

$$P_d\left\{[(\bar{\sigma}_m)_1]^{(z)}_{n+1}\right\} = 1 - \exp\left[-\left(\frac{[(\bar{\sigma}_m)_1]^{(z)}_{n+1}}{S_o}\right)^M\right]$$

(v) Compute volume fractions:

$$(\phi_3)^{(z)}_{n+1} = \phi \cdot P_d\{[(\bar{\sigma}_m)_1]^{(z)}_{n+1}\} = \phi \cdot \left\{1 - \exp\left[-\left(\frac{[(\bar{\sigma}_m)_1]^{(z)}_{n+1}}{S_o}\right)^M\right]\right\},$$

$$(\phi_1)^{(z)}_{n+1} = \phi - (\phi_3)^{(z)}_{n+1}$$

(vi) Perform convergence check:

If $\left|\frac{(\phi_1)^{(z)}_{n+1} - (\phi_1)^{(z-1)}_{n+1}}{(\phi_1)^{(z-1)}_{n+1}}\right| \leq TOL$ (e.g., 10^{-8}): then update quantities in (iii), (v)

$$(E_*)_{n+1} = (E_*)^{(z)}_{n+1},\ (\nu_*)_{n+1} = (\nu_*)^{(z)}_{n+1};\ [(\bar{\sigma}_{ii})_1]_{n+1} = [(\bar{\sigma}_{ii})_1]^{(z)}_{n+1},\ (i = 1, 2, 3);$$

$$(\phi_1)_{n+1} = (\phi_1)^{(z)}_{n+1},\ (\phi_3)_{n+1} = (\phi_3)^{(z)}_{n+1}; \quad \text{EXIT.}$$

Otherwise: SET $z = z + 1$; GO TO (iii).

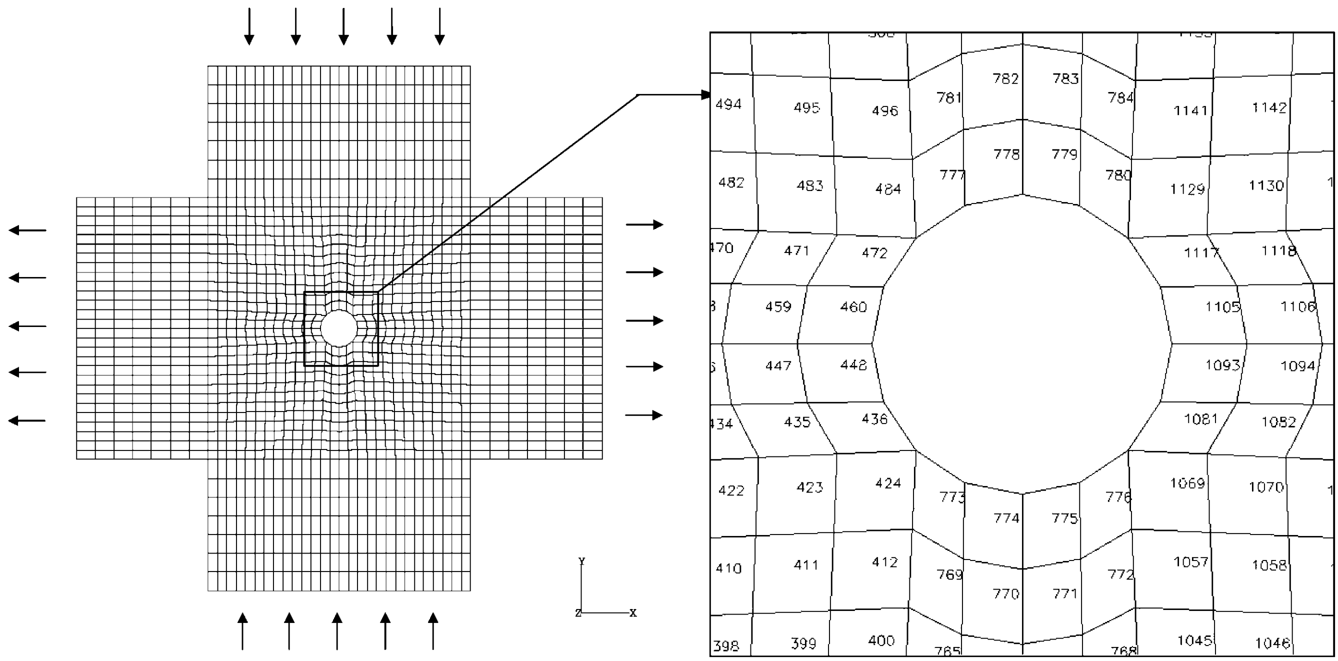

Fig. 5. Finite element discretization employed to simulate the damage evolution of cruciform shaped specimen during biaxial loading

4.2
Four-point bend impact simulations

In crush tests of automotive composite tubes, flexural properties and the corresponding damage mechanisms of components must be characterized. A four-point bend test, which is suitable for high-strength materials, is commonly used for determining the flexural properties of high-strength composites. To assess the predictive capability of the computational model for addressing the impact damage of composite structures, numerical four-point bend impact simulations are carried out. The composite plate, loading noses, and supports are modeled based on ASTM D 790 developed for determining the flexural properties of chopped fiber-reinforced plastics. In order to avoid excessive indentation, or failure due to stress concentration directly under the loading nose, the arc of the loading nose in contact with the specimen must be sufficiently large to prevent contact of the specimen with the sides of the nose. In DYNA3D program this requirement is satisfied by specifying the rigid loading noses and rigid supports as the master surface and the set of nodes on the composite plate as the slave contact node set. The nodes of the loading noses are given at an initial velocity of 8.6 m/s in the negative direction. The default DYNA3D shell element formulation based on Belyschko–Tsay theory is utilized for modeling the composite plate. We employ the same material parameters for the composites as those used in the simulations for a biaxial test.

Figure 8 shows the sequence of damage contours and deformed shape during four-point bend impact, showing a maximum damage at the surface of the composite plate around loading noses. Time history plots for the damage index ϕ_3 at the contact surfaces of the composite plate around loading noses and at the center between loading noses and supports are shown in Fig. 9. It is observed from Figs. 8 and 9 that the implemented computation model can be used for predicting impact damage evolution of composite structures. Specifically, more four-point bend impact simulations will be performed with a geometrical trigger at the center of the plate to characterize the constitutive response and damage evolution of composite structures under crush.

4.3
Parametric study of Weibull parameter S_o

Weibull parameter S_o given in Eq. (19) is related to the interfacial strength between fibers and the matrix. To illustrate the influence of Weibull parameter S_o on the damage evolution in composite materials and evaluate constitutive model sensitivity to Weibull parameter S_o, parametric analysis is carried out. As a debonding property of the fiber-matrix interface, four sets of the Weibull parameters are used: $S_o = 0.109 * 150$ MPa and $M = 4$; $S_o = 0.80 * 150$ MPa and $M = 4$; $S_o = 1.09 * 150$ MPa and $M = 4$; and $S_o = 10.9 * 150$ MPa and $M = 4$. For comparison, four-point bend impact simulations are conducted using the same finite element model as used in four-point bend impact simulations. We plot time history for the volume fraction of perfectly bonded fibers ϕ_1 for various values of Weibull parameter S_o at the contact surface of the composite plate around loading noses during four-point bend impact in Fig. 10. As shown in Fig. 10, if the interfacial strength between fibers and the matrix is low (lower S_o), most fibers are debonded in early stage and the material will show the nonlinear behavior. It is concluded from the parametric study that the influence of Weibull parameter S_o on the constitutive behavior and damage evolution of the composite is quite remarkable;

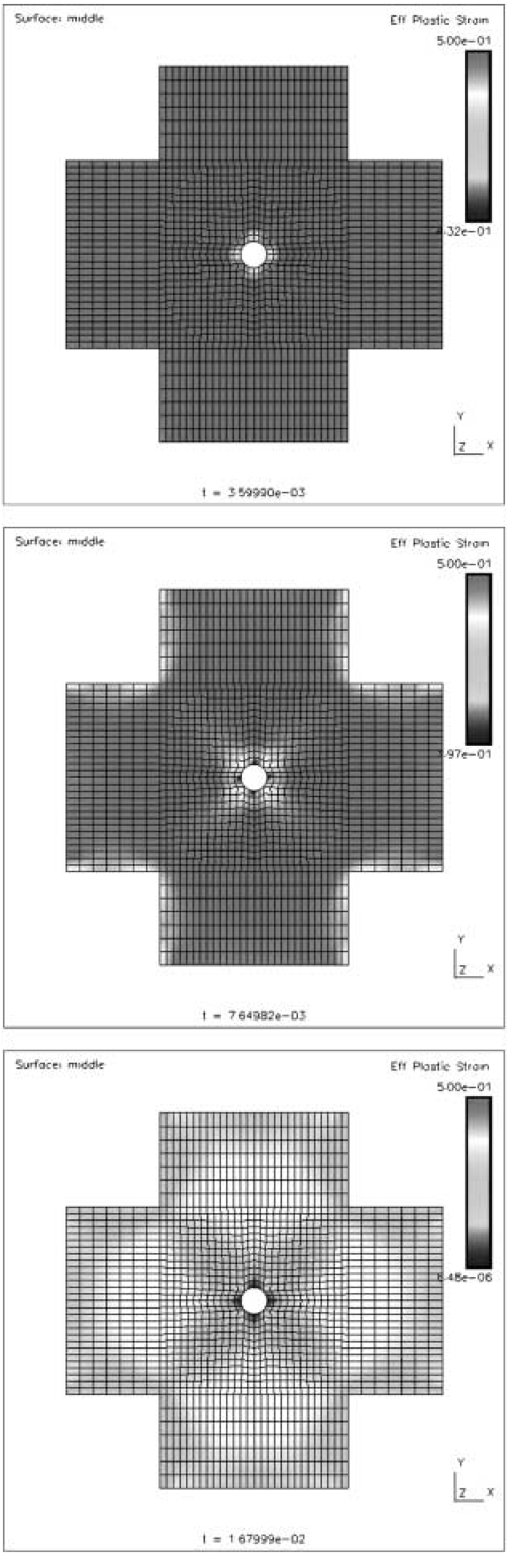

Fig. 6. The sequence of damage contours during biaxial loading, showing the damage zone emanating from the edges of the cutout

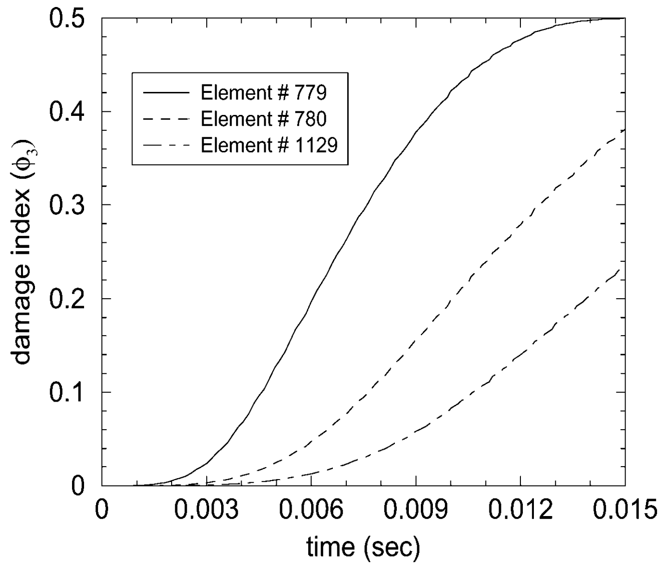

Fig. 7. Time history plots for ϕ_3 around the cutout of composite specimen during biaxial loading

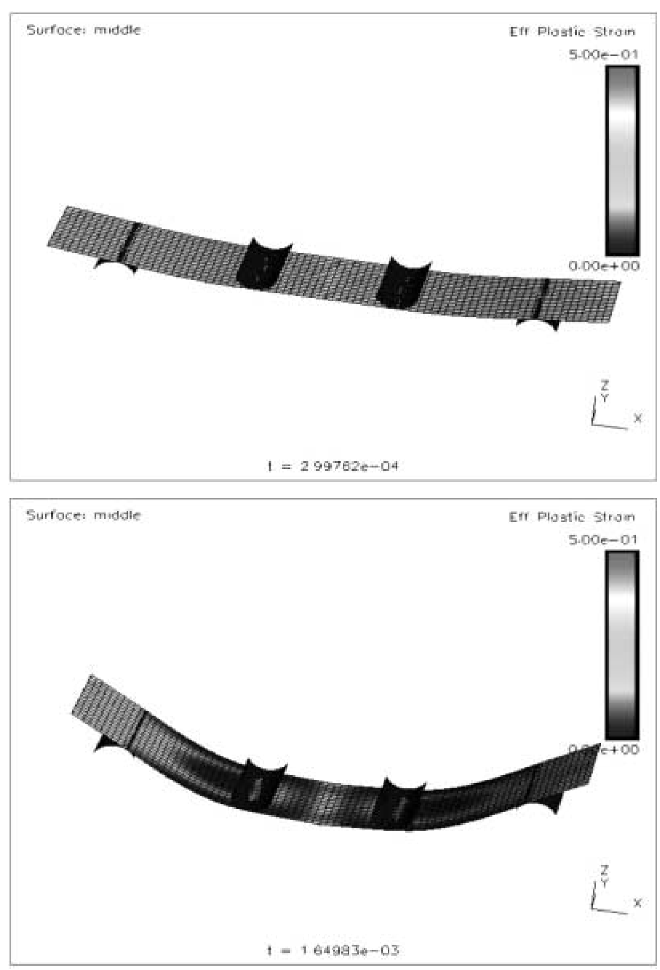

Fig. 8. The sequence of damage contours and deformed shape of composite plate during four-point bend impact

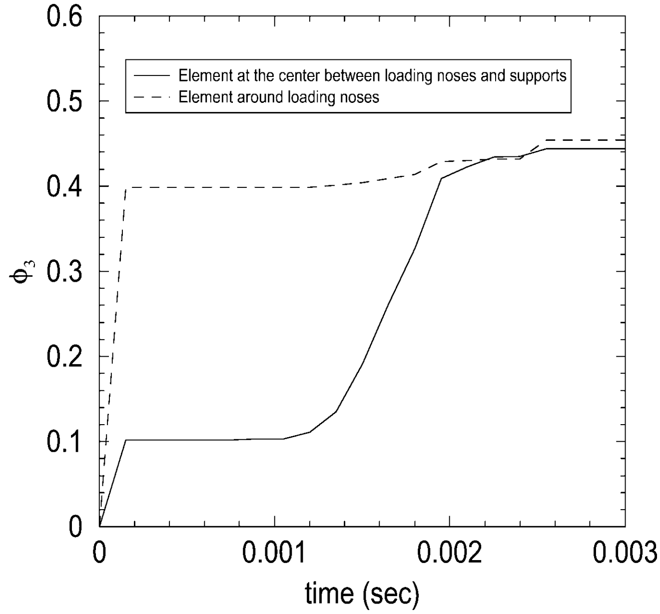

Fig. 9. Time history plots for ϕ_3 at the contact surfaces of composite plate around loading noses and at the center between loading noses and supports during four-point bend impact

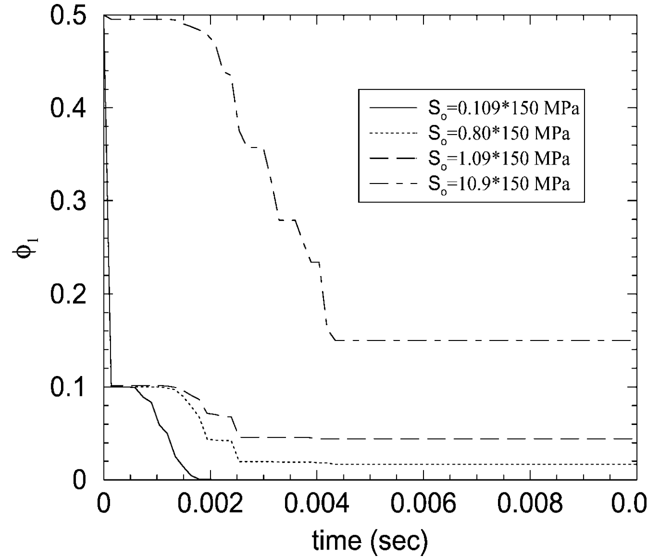

Fig. 10. Time history plots for ϕ_1 for various values of Weibull parameter S_o at the contact surface of composite plate around loading noses during four-point bend impact

therefore, further laboratory experiment is needed to determine the Weibull (damage) parameters.

5
Concluding remarks

Emanating from a constitutive damage model for aligned fiber-reinforced composites, a micromechanical damage constitutive model was developed to perform impact simulation of randomly oriented, discontinuous fiber-reinforced composites. Evolutionary interfacial debonding model and a crack-weakened model were subsequently employed in accordance with the Weibull's probability function to characterize the varying probability of fiber debonding. By adding the corresponding inclusion phases, the extension of the constitutive model to predict the mechanical behavior of new composite materials (e.g. Programmable Powder Preform) in which discontinuous carbon fibers are deposited on the preform with precise spatial and orientation distributions containing cracks of different sizes and orientations is possible.

In the derivation, the analogy for the equivalence between partially debonded fibers and the transversely isotropic perfect spheroids was valid only for uniaxial loading. Although the current approach can deal with partial debonding on different fiber location by adding the corresponding equivalent inclusion appropriately, the implementation of different partial debonding results in expensive finite element simulations. However, the extension of the current formulation to be able to deal with different partial debonding is straightforward. Further, fiber debonding was considered as a primary damage mechanism under impact. However, increasing the crushing speed in fiber-matrix composites automatically influences the failure phenomena, and failure type can evolve from being fiber debond dominated to one that is dominated by matrix cracking. Therefore, the model will be extended to be able to accommodate the necessary failure mechanisms under impact in a forthcoming paper.

The constitutive damage model was then implemented into a finite element program DYNA3D to simulate the dynamic behavior and the progressive damage of composite materials. Numerical simulations for a biaxial loading test and a four-point bend impact test of composite specimens were carried out to validate the computational model and investigate impact damage evolution in discontinuous fiber-reinforced composite structures. Furthermore, parametric analysis was performed to address the influence of Weibull parameter on the damage evolution in composites. Based on the numerical simulations and parametric study, we can draw the conclusion that although more experimental work is needed to determine the damage parameters, the implementation of a new constitutive model into the finite element code DYNA3D has resulted in a promising numerical tool for the simulation of progressive damage in impacted composite structures.

Appendix
Parameters $\tau_1, \ldots, \tau_6$ in Eq. (7)

These parameters take the form:

$$\tau_1 = 2\mu_0 \sum_{r=1}^{3} (m_r)_1$$

$$\tau_2 = 2\mu_0 \sum_{r=1}^{3} (m_r)_2$$

$$\tau_3 = \lambda_0 \sum_{r=1}^{3} [(m_r)_1 + 4(m_r)_2 + 3(m_r)_3] + 2\mu_0 \sum_{r=1}^{3} (m_r)_3$$

$$\tau_4 = 2\mu_0 \sum_{r=1}^{3} (m_r)_4$$

$$\tau_5 = \lambda_0 \left\{ 1 + \sum_{r=1}^{3} [(m_r)_4 + 3(m_r)_5 + 2(m_r)_6] \right\} + 2\mu_0 \sum_{r=1}^{3} (m_r)_5 \tag{22}$$

$$\tau_6 = 2\mu_0 \left[\frac{1}{2} + \sum_{r=1}^{3} (m_r)_6 \right]$$

in which $(m_r)_1, \ldots, (m_r)_6$ are the parameters of the fourth-rank tensor $\tilde{F}_{ijkl}[(m_r)_1, \ldots, (m_r)_6]$, which is the product between $\tilde{F}_{ijkl}[\phi_1(b_r)_1, \ldots, \phi_1(b_r)_6]$ and $\tilde{F}_{ijkl}[(l_r)_1, \ldots, (l_r)_6]$. $\tilde{F}_{ijkl}[(l_r)_1, \ldots, (l_r)_6]$ is the inverse of $\tilde{F}_{ijkl}[(j_r)_1, \ldots, (j_r)_6]$ with the following parameters

$$\begin{aligned}
(j_r)_1 &= \phi_r\{-(S_r)_1[(b_r)_1 + 4(b_r)_2 + (b_r)_3 + 2(b_r)_6] \\
&\quad - 4(S_r)_2[(b_r)_1 + 2(b_r)_2 + (b_r)_3] \\
&\quad - (S_r)_4[(b_r)_1 + 4(b_r)_2 + 3(b_r)_3] - 2(S_r)_6(b_r)_1\} \\
(j_r)_2 &= \phi_r\{-2(S_r)_2[(b_r)_2 + (b_r)_6] - 2(S_r)_6(b_r)_2\} \\
(j_r)_3 &= \phi_r\{-(S_r)_3[(b_r)_1 + 4(b_r)_2 + (b_r)_3 + 2(b_r)_6] \\
&\quad - (S_r)_5[(b_r)_1 + 4(b_r)_2 + 3(b_r)_3] \\
&\quad - 2(S_r)_6(b_r)_3\} \\
(j_r)_4 &= \phi_r\{-(S_r)_1[(b_r)_4 + (b_r)_5] - 4(S_r)_2[(b_r)_4 + (b_r)_5] \\
&\quad - (S_r)_4[(b_r)_4 + 3(b_r)_5 + 2(b_r)_6] - 2(S_r)_6(b_r)_4\} \\
(j_r)_5 &= \phi_r\{-(S_r)_3[(b_r)_4 + (b_r)_5] - (S_r)_5[(b_r)_4 + 3(b_r)_5 \\
&\quad + 2(b_r)_6] - 2(S_r)_6(b_r)_5\} \\
(j_r)_6 &= \frac{1}{2} - \phi_r[2(S_r)_6(b_r)_6]
\end{aligned} \tag{23}$$

In addition, $(b_r)_1, \ldots, (b_r)_6$ are the parameters of the fourth-rank tensor $\tilde{F}_{ijkl}[(b_r)_1, \ldots, (b_r)_6]$, which is the inverse of $\tilde{F}_{ijkl}[(d_r)_1, \ldots, (d_r)_6]$ with the following parameters

$$\begin{aligned}
&(d_1)_1 = (S_1)_1,\ (d_1)_2 = (S_1)_2, \\
&\qquad (d_1)_3 = (S_1)_3,\ (d_1)_4 = (S_1)_4, \\
&(d_1)_5 = \frac{1}{3}\left(\frac{\kappa_0}{\kappa_1 - \kappa_0} - \frac{\mu_0}{\mu_1 - \mu_0} \right) + (S_r)_5, \\
&(d_1)_6 = \frac{1}{2} \frac{\mu_0}{\mu_1 - \mu_0} + (S_1)_6
\end{aligned} \tag{24}$$

$$\begin{aligned}
&(d_2)_1 = 2e_1\mu_0 + (S_2)_1,\ (d_2)_2 = 2e_2\mu_0 + (S_2)_2, \\
&(d_2)_3 = 2e_3\mu_0 + (S_2)_3, \\
&(d_2)_4 = e_1\lambda_0 + 4e_2\lambda_0 + 2e_4\mu_0 + (S_2)_4, \\
&(d_2)_5 = e_3\lambda_0 + 2e_5\mu_0 + 2e_6\lambda_0 + (S_2)_5, \\
&(d_2)_6 = 2e_6\mu_0 + (S_2)_6
\end{aligned} \tag{25}$$

$$\begin{aligned}
&(d_3)_1 = (S_3)_1,\ (d_3)_2 = (S_3)_2, \\
&(d_3)_3 = (S_3)_3,\ (d_3)_4 = (S_3)_4, \\
&(d_3)_5 = (S_3)_5,\ (d_3)_6 = -\frac{1}{2} + (S_3)_6
\end{aligned} \tag{26}$$

where $e_1, \ldots, e_6$ in Eq. (25) are the parameters of the fourth-rank tensor $\tilde{F}_{ijkl}[e_1, \ldots, e_6]$, which is the inverse of $\tilde{F}_{ijkl}[f_1, \ldots, f_6]$ with the following parameters

$$\begin{aligned}
f_1 &= \frac{9\mu_1\kappa_1}{3\kappa_1 + 4\mu_1} + \mu_1 \\
f_2 &= -\mu_1 \\
f_3 &= -\frac{9\mu_1\kappa_1}{3\kappa_1 + 4\mu_1} + \mu_1 \\
f_4 &= -\frac{9\mu_1\kappa_1}{3\kappa_1 + 4\mu_1} + \mu_1 \\
f_5 &= \frac{9\mu_1\kappa_1}{3\kappa_1 + 4\mu_1} - \mu_1 - \lambda_0 \\
f_6 &= \mu_1 - \mu_0
\end{aligned} \tag{27}$$

References

1. **Flom Y, Arsenault RJ** (1986) Interfacial bond strength in an aluminium alloy 6061-SiC composite. Materials Science and Engineering 77: 191–197
2. **Goan JC, Prosen SP** (1969) Interfacial bonding in graphite-resin composites. American Society for Testing and Materials. STP 452, 3
3. **Ju JW, Chen TM** (1994a) Micromechanics and effective moduli of elastic composites containing randomly dispersed ellipsoidal inhomogeneities. Acta Mechanica 103: 103–121
4. **Ju JW, Chen TM** (1994b) Effective elastic moduli of two-phase composites containing randomly dispersed spherical inhomogeneities. Acta Mechanica 103: 123–144
5. **Ju JW, Lee HK** (2000) A micromechanical damage model for effective elastoplastic behavior of ductile matrix composites considering evolutionary complete particle debonding. Comp. Meth. Appl. Mech. Eng. 183: 201–222
6. **Lee HK** (1998) Three-dimensional Micromechanical Damage Models for Effective Elastic and Elastoplastic Behavior of Composite Materials with Inhomogeneities or Microcracks. Ph.D. Thesis, University of California at Los Angeles
7. **Lee HK, Simunovic S** (2000) Modeling of progressive damage in aligned and randomly oriented discontinuous fiber polymer matrix composites. Composites Part B: Eng. 31: 77–86
8. **Lee HK, Simunovic S** (2001) A damage constitutive model of progressive debonding in aligned discontinuous fiber composites. Int. J. Solids Struct. 38: 875–895
9. **Ochiai S, Osamura K** (1988) Influence of Interface on Fracture Behavior and Strength of Unnotched Unidirectional Metal Matrix Composites. Proc. 2nd Int. Conf. on Composite Interfaces (ICCI-II), pp. 413–423
10. **Rondeau R, Reeve S, Bond G** (1999) Effect of Tows and Filament Groups on the Properties of Discontinuous Fiber Composites. Int. SAMPE Symp. Exhibition (Proceedings). 44(II), pp. 1449–1460
11. **Tohgo K, Weng GJ** (1994) A progressive damage mechanics in particle-reinforced metal-matrix composites under high triaxial tension. J. Eng. Mater. Tech. 116: 414–420
12. **Waas AM, Quek SC** (1999) Biaxial testing of fiber-reinforced composites-implications for numerical tools in crash energy management. Final Report to the ACC, University of Michigan
13. **Zhao YH, Weng GJ** (1996) Plasticity of a two-phase composite with partially debonded inclusions. Int. J. Plasticity 12: 781–804
14. **Zhao YH, Weng GJ** (1997) Transversely isotropic moduli of two partially debonded composites. Int. J. Solids Struct. 34: 493–507